Final Draft
of the original manuscript:

Du, B.; Handge, U.A.; Wambach, M.; Abetz, C.; Rangou, S.; Abetz. V.:
Functionalization of MWCNT with P(MMA-co-S) copolymers via ATRP: Influence on localization of MWCNT in SAN/PPE 40/60 blends and on rheological and dielectric properties of the composites
In: Polymer (2013) Elsevier

DOI: 10.1016/j.polymer.2013.08.065

Functionalization of MWCNT with P(MMA-*co*-S) copolymers via ATRP: Influence on localization of MWCNT in SAN/PPE 40/60 blends and on rheological and dielectric properties of the composites

Bing Du [a], Ulrich A. Handge [a], Mona Wambach [a], Clarissa Abetz [a], Sofia Rangou [a], Volker Abetz [a, b, *]

[a] Institute of Polymer Research, Helmholtz-Zentrum Geesthacht
Max-Planck-Strasse 1, 21502 Geesthacht, Germany

[b] Institute of Physical Chemistry, University of Hamburg
Grindelallee 117, 20146 Hamburg, Germany

Abstract

In this work, the localization of functionalized multi-walled carbon nanotubes (MWCNT) with random copolymers of methyl methacrylate and styrene (P(MMA-*co*-S)) in poly(styrene-*co*-acrylonitrile)/poly(2, 6-dimethyl-1, 4-phenylene ether) blends (SAN/PPE) and its influences on morphological, rheological and dielectric properties of the composites were investigated. P(MMA-*co*-S) copolymers were grafted onto MWCNT via atom transfer radical polymerization (ATRP). The molecular weight of the copolymers was adjusted by controlling the time of reaction. In SAN/PPE blends, MWCNT grafted with low molecular weight copolymers were predominantly located at the interface of the blend and a few individual tubes were dispersed in the PPE phase. Aggregation of MWCNT was observed nearby the interfacial region because of micellization of grafted copolymers. Aggregation was more pronounced with increasing molecular weight of the grafted P(MMA-*co*-S) copolymer. In the melt, the composite containing MWCNT with low molecular weight copolymers had higher dynamic moduli than the one with pristine MWCNT. An increasing molecular weight of grafted copolymer led to a softening effect which resulted in a reduction of the moduli of the composite. Although a pronounced enhancement was observed for the composites with pristine MWCNT, only a small increase in electrical conductivity was achieved by adding functionalized MWCNT owing to the poor network formed by functionalized MWCNT in the blends.

Keywords: SAN/PPE blends, multi-walled carbon nanotubes, random copolymers, rheology

*Corresponding author. Tel.: +49 4152 87 2461; fax: +49 4152 87 2499.
E-mail address: volker.abetz@hzg.de

1. Introduction

Nanocomposites based on phase separated polymer blends have attracted increasing interest in the last two decades. Elias et al. [1] successfully used silica nanoparticles as stabilizers to suppress the coalescence of droplets in polypropylene/poly(ethylene-*co*-vinyl acetate) (PP/EVA) immiscible blends. Compatibilization of a polycarbonate/poly(methyl methacrylate) blend was realized by adding a specific organoclay [2]. In composites based on a high-density polyethylene/ poly(ethylene-*co*-vinyl acetate) (HDPE/EVA) blend, graphite nanosheets selectively located in the HDPE phase and considerably increased the electrical conductivity of the immiscible blend at a filler loading of 10 wt% [3]. Among several kinds of nanofillers, CNT with outstanding properties have shown a promising potential to improve the mechanical strength, electrical and thermal conductivity of polymer composites, since the use of carbon nanotubes (CNT) as fillers in polymer matrices was reported for the first time in 1994 by Ajayan et al. [4]. In contrast to composites based on homopolymers, a lower percolation threshold can be achieved by filling CNT into immiscible blends because of selective location of CNT in one specific phase of the blends. This concept is known as “double percolation” which implies the percolation of the CNT filled phase in the blend and the additional percolation of the CNT in the percolated phase [5-10]. Besides of this remarkable effect on electrical conductivity, the addition of CNT also has a significant influence on the morphology of immiscible blends. Zou et al. [11] prepared a series of nanocomposites based on poly(*p*-phenylene sulfide)/polyamide 66 (PPS/PA 66) blends with different loadings of multi-walled carbon nanotubes (MWCNT). In their work, MWCNT were selectively located in the PA 66 phase and the morphology of the blends varied with loading of MWCNT. For a low concentration of MWCNT, well-dispersed MWCNT formed a network-like structure and were in contact with each other, promoting the PA 66 droplets to coalesce into a quasi-continuous phase. Consequently, the droplet structure of PPS/PA 66 blends transferred to a co-continuous structure in the presence of low amount of MWCNT. With increasing MWCNT loading, the MWCNT in the PA 66 phase tended to aggregate. This effect induced a formation of PA 66 spheres. In this case, the morphology of the blends formed a droplet structure with a larger size of dispersed PA 66 domains. In the work of Wu et al. [9], a morphological change of

poly(ε-caprolactone)/polylactide blends (PCL/PLA) was also found with a reduction of dispersed PLA domains. The well dispersed pristine MWCNT which were selectively located in the PCL phase increased the viscosity of the PCL phase leading to a break-up of the dispersed PLA droplets.

In the abovementioned examples, the CNT were all selectively located in one specific phase. By combining the experimental results of polycarbonate/poly(styrene-*co*-acrylonitrile)/MWCNT (PC/SAN/MWCNT) composites with the theoretical investigations of Krasovitsky and Marmur [12], Göldel et al. [5] concluded that localization of CNT with an extremely high aspect ratio at the interface is highly improbable and the nanotubes prefer to be located in the selective phase with a more pronounced wetting between CNT and the surrounding polymer. However, the location at the interface possibly is an ideal situation in order to maximize the improving effect of CNT on the properties of immiscible blends. If the CNT are located at the interface in a blend with a co-continuous phase morphology, electrical percolation can be achieved with the lowest loading due to the so-called “triple percolation” [13]. Compatibilization of immiscible blends can be also realized by the addition of CNT at the interface. Thus, it is essential to study and develop approaches of confining CNT at the interface of multi-phase blends.

Until now, only a few successful examples were reported where CNT were selectively located at the interface in multi-phase blends. Very recently, Baudouin et al. [14] demonstrated the possibility to confine pristine MWCNT at the interface for the first time in blends of polyamide and poly(ethylene-*co*-alkyl acrylate) copolymers (EA) through applying a specific mixing strategy. A more general method is to pre-functionalize CNT before the filling procedure. Wu et al. [9] improved the properties of PCL/PLA blends by adding carboxylic MWCNT. Since the carboxylic group had a good affinity with both PCL and PLA, some fractions of functionalized MWCNT were found to concentrate at the interface of the blends, while unfunctionalized tubes were located in the PCL matrix which had a lower viscosity than PLA. Bose et al. [15, 16] modified MWCNT by styrene-maleic anhydride copolymers (SMA) and the functionalized MWCNT were used as reactive compatibilizers locating at the interface of blends of PA 6 and acrylonitrile–butadiene–styrene copolymer (ABS). The work of Chen and his coworkers [17]

reported an improvement of the interfacial adhesion of HDPE/PA 6 composites with functionalized MWCNT. Their work gave direct evidence that the fracture toughness of immiscible polymer blends can be enhanced by MWCNT which are selectively located at the interface. However, the authors designed a particular way to realize the localization at the interface. The composites were formed by merging three different polymer sheets together in turn with a tailored order and MWCNT were only pre-filled into the polymer sheet which was arranged as the middle layer of the composites.

Regarding to immiscible blends prepared by melt processing, many experimental and theoretical results were devoted to the strategy of using random copolymers as compatibilizers which contain the same monomeric or miscible units as the components of blends [18-20]. Random copolymers at the interface can enhance the interfacial adhesion [20, 21] and reduce the interfacial tension between the blend phases [22]. Besides, compared to traditional compatibilizers such as block or graft copolymers, synthesis of random copolymers is more facile and less expensive [21]. Thus, in this work, we attempted to locate MWCNT at the interface by grafting a random copolymer on the surface of MWCNT. Since the copolymers containing poly(methyl methacrylate) (PMMA) and polystyrene (PS) are good compatibilizers for poly(styrene-*co*-acrylonitrile)/poly(2, 6-dimethyl-1, 4-phenylene ether) (SAN/PPE) blends [23-25], we modified MWCNT with random copolymers of PMMA and PS via atom transfer radical polymerization (ATRP). In the blends, the weight ratio of SAN and PPE was 40 to 60, as optimum mechanical properties of SAN/PPE 40/60 blends were reported [23]. The grafted copolymer groups on the surface of MWCNT were expected to promote MWCNT to be selectively located at the interface. Furthermore, the influence of grafted polymer on the rheological properties and electrical conductivity as well as the permittivity of the composites was studied in our work.

2. Experiments

2.1 Materials

Poly(styrene-*co*-acrylonitrile) (SAN, Luran® 358N) used in this work was provided by BASF SE

(Ludwigshafen, Germany) in granular form with a weight-average molecular weight of 161000 g/mol and a polydispersity index (PDI) of 1.95. The content of acrylonitrile was 25 wt% which led to a miscibility between SAN and PMMA during melt processing. Poly(2,6-dimethyl-1,4-phenylene ether) (PPE, PX100F) powder was supplied by Mitsubishi Engineering Plastics Europe (Düsseldorf, Germany), having a weight-average molecular weight of 28000 g/mol and a PDI of 2.42. The molecular weights of both SAN and PPE were characterized by gel permeation chromatography (GPC) using an UV detector relative to polystyrene at 30 °C. In order to protect PPE from oxidation, a mixture of Irganox 1010 and Irgafos 168 (Sigma Aldrich, Schnelldorf, Germany) was used as stabilizers with a concentration of 0.1 wt% during melt processing. The ratio of Irganox 1010 to Irgafos 168 was 2.

The reagents of methyl methacrylate (≥99%), styrene (≥99%), 2-bromo-2-methylpropionyl bromide (2BriBr, 99%), triethyl amine (TEA, ≥99.5%), copper (I) chloride (CuCl, ≥99%), copper (II) chloride ($CuCl_2$, ≥99%) and N, N, N', N', N-pentamethyl diethylenetriamine (PMDETA, 97%) were purchased from Sigma-Aldrich (Schnelldorf, Germany). The solvents of tetrahydrofurane (THF), chloroform ($CHCl_3$), anisole and methanol were used as received.

Pristine MWCNT and amino functionalized MWCNT (MWCNT-NH_2) were obtained from FutureCarbon GmbH (Bayreuth, Germany) with a purity of >90 % and a diameter of ~15 nm. The length of MWCNT was in the range of 10-50 μm. The number of walls of MWCNT was about 10 and the specific surface area of MWCNT was around 250 m^2/g [26, 27].

2.2 Anchoring initiator onto the surface of MWCNT

The procedure of anchoring initiator onto MWCNT followed the work reported by Ryu et al. [28]. It is worth noting that we significantly increased the scale of the reaction in order to prepare a sufficient amount of functionalized nanotubes in one batch for extrusion. In our up-scaled reaction, 9.6 g as-received MWCNT-NH_2 were dispersed in THF (1.156 L) by treating in an ultrasonication bath for 5 min. Then the suspension was vigorously stirred under argon flow before dropwise adding 40 ml TEA. Afterwards, the system was further degassed by switching between the vacuum and the argon flow thrice. The anchoring reaction was produced after

injecting a diluted solution of 2BriBr (32 ml) in THF (160 ml) at 0 °C. Subsequently, the mixture was still kept stirring at such low temperature for 2 hours and heated up at ambient temperature for 48 hours. When the reaction was completed, the black solid was separated and washed by chloroform for several times until no green filtrate was observed. Lastly, the obtained MWCNT with initiator (MWCNT-Br) was dried in an oven under vacuum at room temperature for one week.

2.3 Polymerization of P(MMA-*co*-S) random copolymers on the surface of MWCNT

In a typical reaction, 500 mg MWCNT-Br were dispersed in a liquid mixture of 8.7 ml MMA, 9.3 ml styrene and 18 ml anisole. After being treated by ultrasonication for 5 minutes, 0.5 mol% copper salts (with respect to the total amount of monomers, including CuCl and $CuCl_2$ with a weight ratio of 0.8 to 0.2) were added. Then, the system was vigorously stirred under argon atmosphere for one hour. Once 0.5 mol% PMDETA (with respect to the total amount of monomers) was fed, the flask was rapidly moved into an oil bath with a temperature of 125 ºC. After a desired reaction time, the product was precipitated in methanol and washed by THF for several times to dissolve the free polymers which were unanchored on MWCNT. Before filling into the polymeric matrix, the functionalized MWCNT were dried in an oven under vacuum at room temperature for one week. In order to obtain functionalized MWCNT with different molecular weight of copolymers, most reaction parameters in different reactions were unaltered, whereas, only the time of each reaction varied. The conditions for preparing functionalized MWCNT are listed in Table 1.

Table 1 Reaction conditions for functionalization of MWCNT with P(MMA-*co*-S) random copolymers via ATRP

Sample	Temperature [ºC]	Monomer: CuCl: $CuCl_2$: PMDETA: Initiator [molar ratio]	MMA : Styrene [molar ratio]	Reaction Time
MWCNT-*CO*-3h	125	200:0.8:0.2:1:0.25	1 : 1	3 h
MWCNT-*CO*-4h	125	200:0.8:0.2:1:0.25	1 : 1	4 h
MWCNT-*CO*-5h	125	200:0.8:0.2:1:0.25	1 : 1	5 h
MWCNT-*CO*-6h	125	200:0.8:0.2:1:0.25	1 : 1	6 h
MWCNT-*CO*-7h	125	200:0.8:0.2:1:0.25	1 : 1	7 h

2.4 Preparation of SAN/PPE composites filled with MWCNT

The procedure of preparation of SAN/PPE composites filled with MWCNT is schematically shown in Fig. 1. The given amount of MWCNT fillers was sonicated in chloroform by an ultrasonic probe (Bandelin SONOPULS, frequency of 20 kHz, 60 W) for 30 minutes and an ultrasonic bath (Bandelin SONOREX, frequency of 35 kHz, 160 W) for 1 hour. Then commercial SAN pellets and PPE powders were fed into the system with a weight ratio of 40 to 60. The concentration of the polymeric mixture in chloroform was 5 wt% and the effective loading of MWCNT (calculated without the content of grafted copolymers) in each sample was 1 wt% with respect to the total amount of SAN and PPE. After vigorously stirring for 24 h, the suspension was directly cast in Teflon® moulds and heated up to 40 °C for one day. In order to evaporate the solvent sufficiently, the cast materials were grinded into small powder by an electrical mixer before drying in a vacuum oven. Lastly, the powder of the composites was dried in a vacuum oven at 80 °C for three weeks.

The specimens for rheological and dielectric measurements were prepared by melt processing. The dried composites with MWCNT were extruded using a micro-compounder with a filling volume of 15 cm^3 (DSM Xplore, Geleen, Netherlands) at 260 °C. The speed of revolutions was 100 rpm and the mixing time was 5 minutes. During extrusion, nitrogen flow was introduced into the mixing chamber for minimizing degradation. Then, round disks were formed by using a micro-injection moulding machine with a filling volume of 12 cm^3 (DSM Xplore, Geleen, Netherlands). The temperature in the injection chamber was 280 °C and the mould temperature was set to 100 °C. The pressure for shooting was set to 4 bar for 4 seconds. Moreover, a pressure of 6 bar for 4 seconds was set for further holding process. For comparison, the samples of neat blends were also prepared under the same conditions.

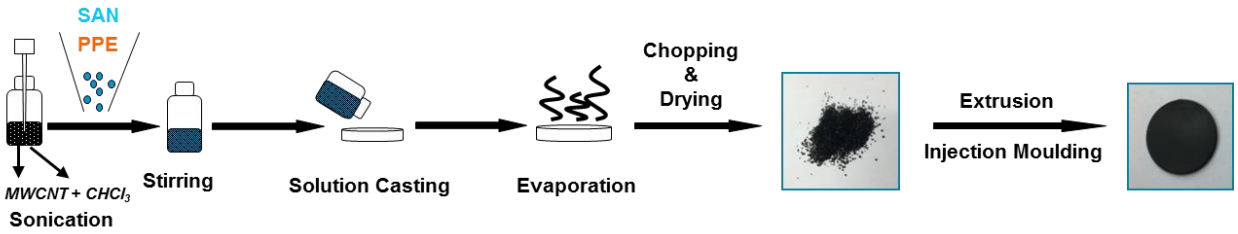

Fig. 1 Scheme of preparation of SAN/PPE 40/60 blends filled with MWCNT

2.5 Characterization

2.5.1 Gel permeation chromatography

The average molecular weight of the neat polymer components and the free copolymers polymerized from ATRP reaction in presence of MWCNT was characterized by gel permeation chromatography (GPC) and analysis by an UV detector using THF as solvent and standard polystyrene (PS) as calibration.

2.5.2 Fourier transform infrared spectra

The Fourier transform infrared spectra (FT-IR) measurements were carried out using a Bruker Equinox 55 (Bruker Optics, Ettlingen, Germany). The MWCNT samples were carefully dispersed in potassium bromide (KBr) and compressed into pellets under high loading. The content of carbon nanotubes in KBr pellets was 0.1 wt% in the case of MWCNT-NH_2 and MWCNT-Br, while, it was 0.5 wt% in the case of functionalized MWCNT with P(MMA-*co*-S) copolymers. The infrared spectra were recorded in a spectral range of 600-3200 cm^{-1} with a spectral resolution of 1 cm^{-1}.

2.5.3 Thermal gravimetric analysis

Thermal gravimetric analysis (TGA) was carried out using a TGA device Netzsch TG209 F1 Iris (Netzsch-Gerätebau GmbH, Selb, Germany). The measurements were conducted at constant argon flow with a flow rate of 20 ml/min. The temperature range was 25 °C to 1000 °C, and the heating rate was 10 °C/min.

2.5.4 Nuclear magnetic resonance spectroscopy

The composition of P(MMA-*co*-S) copolymers was determined by nuclear magnetic resonance spectroscopy (^{1}H-NMR) of the free polymers generated from ATRP reaction in the presence of MWCNT. The measurements were carried out using a Bruker AV-300 (Bruker BioSpin Co. Ltd, Karlsruhe, Germany) at 300 MHz. The solvent for measurements was $CDCl_3$.

2.5.5 Transmission electron microscopy

The morphological properties of composites were characterized by transmission electron

micrographs (TEM) using a Tecnai G2 F20 (FEI) operated at an acceleration voltage of 200 kV in bright field mode. Ultrathin sections with a thickness of about 50 nm-100 nm were cut at room temperature from the injection-molded round disks for rheological experiments by means of a Leica Ultracut UCT microtome (Leica Microsystems, Wetzlar, Germany) equipped with a diamond knife. Afterwards, the ultrathin sections were stained with RuO_4 for 10 min.

2.5.6 Rheological measurements

Prior to measurements, the specimens were dried in a vacuum oven under 80 °C for 24 hours. The measurements were carried out using the rotational rheometer ARES (Rheometrics Scientific, Piscataway, USA) in a parallel-plates configuration with a diameter of 20 mm and a gap of 1.6 mm. All measurements were performed under a nitrogen atmosphere at 260 °C. Before each measurement, the samples were inserted into the preheated plates and annealed for 8 minutes at the measurement temperature. In order to determine the linear viscoelastic region, dynamic strain sweeps were carried out in the range of 1-10% at an angular frequency of 10 rad/s. The viscoelastic properties were characterized through frequency sweeps in the range of 0.01-100 rad/s starting from the largest frequency. The strain amplitude for each measurement was 5%.

2.5.7 Dielectric spectroscopy

Broadband dielectric measurements were performed using an Alpha-AN high resolution dielectric analyzer (Novocontrol Technologies GmbH, Hundsangen). The samples had a disk-like shape with a diameter of 25 mm and a height of approx. 1.57 mm. Two platinum electrodes with diameters of 20 mm and 30 mm were used for the measurements. No additional support for the electrical contact like conductive silver was used. At each temperature, 49 different frequencies in the range of 10^7 Hz up to 10^{-3} Hz were measured. Furthermore, the temperature was increased in increments of 5 °C from 10 °C up to 80 °C, then in increments of 2 °C back to 10 °C. The temperature stabilization time was set to 600 s. Since no influence of the temperature was found in the measured temperature range, only the results at room temperature (20 °C) are presented and discussed in this paper.

3. Results and discussion

3.1 Functionalization of MWCNT with P(MMA-*co*-S) copolymers

In many works, the polymerization of PMMA via ATRP was carried out at a temperature equal or lower than 90 °C. Nevertheless, styrene presented a very low conversion at these temperatures. By comparing the polymerization of styrene at 90 °C and 125 °C respectively, Liu et al. [29] pointed out that a higher temperature (125 °C) and the use of specific catalysts should be the optimum conditions for both MMA and styrene, which were also suitable for synthesizing P(MMA-*co*-S) copolymers. Therefore, in our work, we adapted this high temperature for the ATRP reaction and utilized a similar catalyst system of $CuCl/CuCl_2$/PMDETA. The advantage of using mixed copper salts was to overcome the comparably fast propagation of MMA by the deactivating effect from Cu^{2+} [30] and the halogen exchange between R-Br and CuCl [31-33].

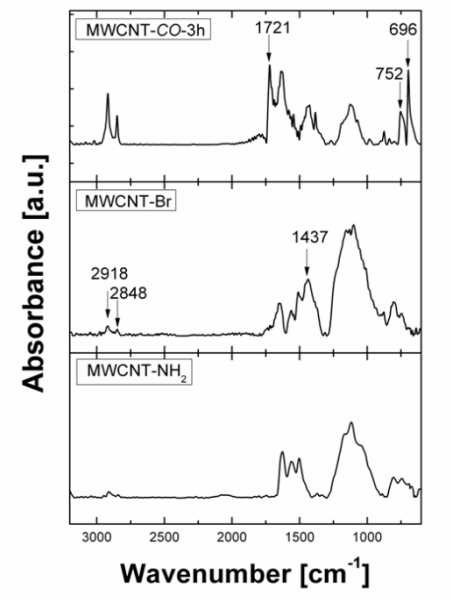

Fig. 2 FT-IR spectra of functionalized MWCNT

Figure 2 shows FT-IR spectra of functionalized MWCNT. For as-received MWCNT-NH_2, the characteristic peaks of the amino group are observed at 1626 cm^{-1} and 1502 cm^{-1} corresponding to N-H deformation [34, 35]. However, many authors also attributed the absorption in the range of 1650 cm^{-1}-1540 cm^{-1} to the C=C stretching mode of the aromatic ring from CNT [36-38]. The broadband absorption locating from 900 cm^{-1} to 1200 cm^{-1} is typical for aromatic systems, which commonly appears in the spectra of covalently functionalized MWCNT [39]. In the case of MWCNT-Br, the presence of initiator is confirmed by the peaks of C-H deformation of alkyl

chains at 1437 cm^{-1}. Moreover, signals from C-H stretching of alkyl groups appear at 2919 cm^{-1} and 2848 cm^{-1} [35], which also proves the existence of the initiator group on MWCNT. In the spectrum of functionalized MWCNT with copolymer (MWCNT-*CO*-3h), the characteristic peaks of nanotubes become weaker. Meanwhile, pronounced signals from grafted polymers are shown with a strong intensity. Successful functionalization of MWCNT with copolymers are determined by the C=O stretching peaks at 1721 cm^{-1} presumably from the ester linkage in MMA units [40] and strong peaks at 752 cm^{-1} and 696 cm^{-1} designated to the out-of-plane bending vibrations of five –CH- groups in the aromatic ring and the out-of-plane skeleton bending vibration of the aromatic ring and respectively from styrene units [41, 42].

The controllability of ATRP reactions for functionalization is examined by investigating the products obtained with different reaction times. Figure 3 shows the TGA results of functionalized MWCNT with copolymers prepared by different reaction times. The as-received MWCNT-NH_2 had a small weight loss of 5.9 wt% corresponding to a concentration of amino groups of 0.64 mmol/g. After the subsequent attachment of 2BriB, the weight loss increases to 12.3 wt%, implying a successful grafting of initiator on the surface of MWCNT with a concentration of 0.403 mmol/g. In the case of functionalized MWCNT with copolymers, the content of grafted copolymers increases from 30 wt% to 80 wt% with a change of total monomer conversion from 35% to 66% (see Fig. 3(b)). These data reveal that the content of grafted copolymers on MWCNT can be adjusted by varying the reaction time or the monomer conversion, which is consistent with the results of functionalizing MWCNT with homopolymers via ATRP [43, 44].

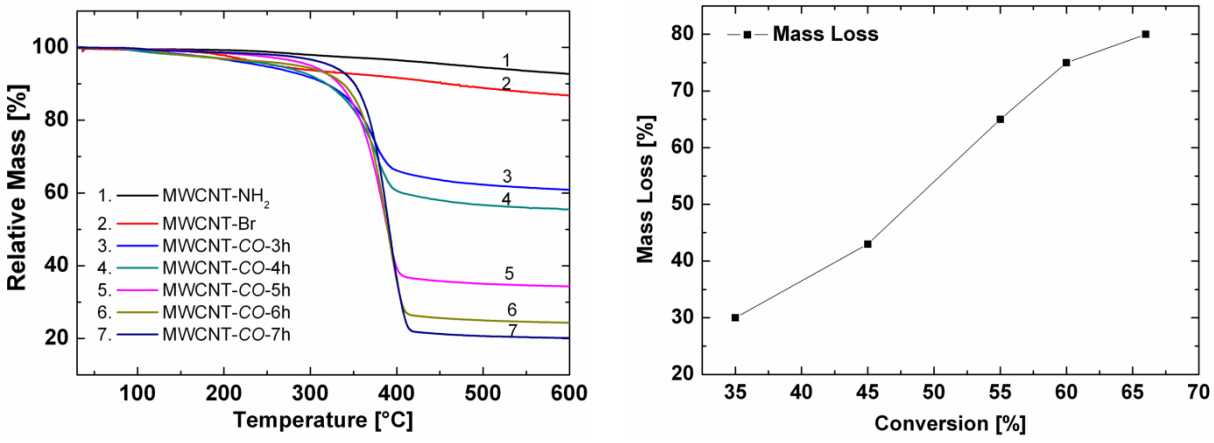

(a) (b)

Fig. 3 TGA curves of MWCNT-NH_2, MWCNT-Br and functionalized MWCNT with P(MMA-*co*-S) copolymers prepared with different reaction times (a) and the content of grafted P(MMA-*co*-S) copolymers as a function of the total monomer conversion (b)

The number-average molecular weight and the PDI as a function of total monomer conversion are shown in Fig. 4. The relationship between the conversion of the total monomers and the molecular weight of copolymers is approximately linear. Furthermore, the PDI remain low (in the range of 1.59 to 1.67) in the obtained conversion range. These characteristics are in agreement with kinetics of normal ATRP reactions in homogenous systems without nanoparticles [45] and are also observed in functionalization of MWCNT reported by other researchers [44]. Based on the aforementioned results, it can be concluded that the ATRP reactions to synthesize P(MMA-*co*-S) copolymers in the presence of MWCNT are characterized by a good controllability under the used conditions. The properties of obtained functionalized MWCNT are summarized in Table 2.

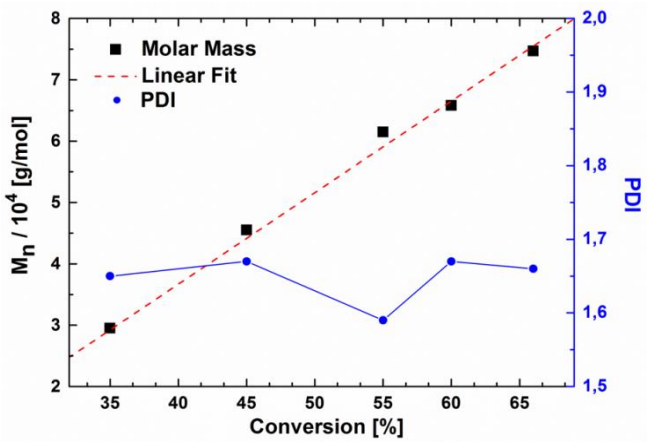

Fig. 4 Number-average molecular weight of P(MMA-*co*-S) copolymers (M_n) and polydispersity index (PDI) as a function of total monomer conversion

Table 2 Summary of characterization of functionalized MWCNT with copolymers

Sample	[Br] [a] [mmol/g]	Conversion of total monomers [b] [%]	Content of grafted polymers[c] [wt%]	M_n [d] [kg/mol]	PDI[d]	Fraction of PS[e] [%]
MWCNT-*CO*-3h	0.403	35	30	29.5	1.65	56%
MWCNT-*CO*-4h	0.403	45	43	45.5	1.67	57%
MWCNT-*CO*-5h	0.403	55	65	61.5	1.59	56%

MWCNT-*CO*-6h	0.403	60	75	65.8	1.67	56%
MWCNT-*CO*-7h	0.403	66	80	74.7	1.66	56%

(a) The concentration of initiator on the surface of MWCNT was calculated using TGA results

(b) The conversion of total monomer mixture was determined by gravimetric weighting

(c) The content of grafted polymer was determined using TGA results of functionalized MWCNT

(d) The number-average molecular weight and polydispersity index of free polymer in the system were measured by GPC using PS as calibration

(e) The fraction of polystyrene component in P(MMA-*co*-S) copolymers was calculated based on the ^{1}H-NMR spectra

The composition of the grafted copolymers was determined from the ^{1}H-NMR spectra of the obtained free polymers during the ATRP reaction. Signals of the main chains and the pendant groups in all spectra are broad and differ significantly from the ones of homopolymers of PMMA and PS [45], illustrating that the obtained polymers are neither block copolymers nor mixture of homopolymers but random copolymers. The compositions of P(MMA-*co*-S) copolymers can be calculated based on the relative areas of aromatic protons (I_1, 6.5-7.25 ppm) corresponding to the styrene units and aliphatic proton region (I_2, 0.3-3.7 ppm) of both units, styrene and MMA units, according to the following equation [45, 46]:

$$\phi_{PS} = \frac{I_1/5}{I_1/5+(I_2-3I_1/5)/8} \quad (1)$$

where ϕ_{PS} is the molar fraction of styrene units in the copolymers. The calculated composition of each grafted copolymer prepared with different reaction times are also listed in Table 2. The results show that the compositions of the copolymers do not depend on the time of polymerization. In fact, the styrene fraction is about 56% in each sample, i.e. slightly larger than the methyl methacrylate fraction. This indicates an almost azeotropic copolymerization, which agrees well with the equal molar concentrations of the comonomers and the similar copolymerization parameters of MMA (r_1=0.46) and styrene (r_2=0.52) [47].

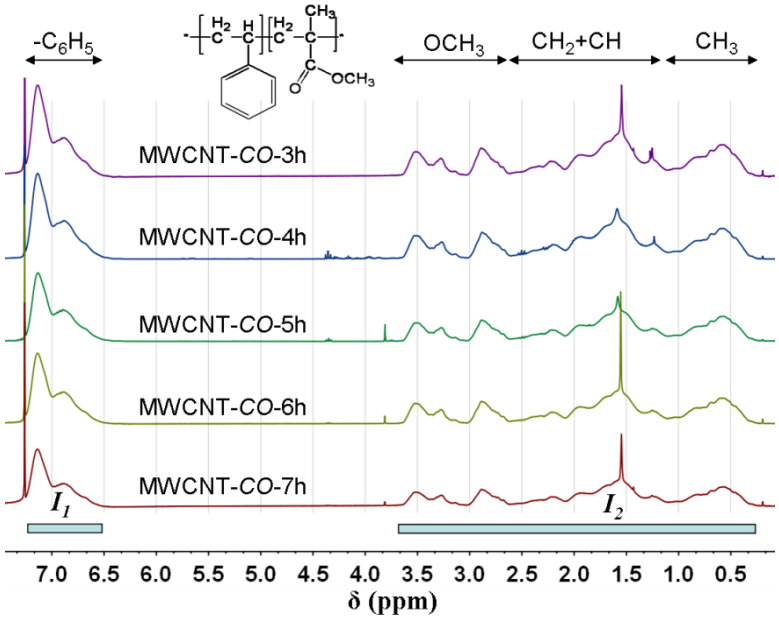

Fig. 5 ^{1}H-NMR spectra of free copolymers polymerized in the presence of MWCNT in $CDCl_3$ at 25°C

3.2 Morphology of SAN/PPE 40/60 blends filled with MWCNT

In order to investigate the influence of the content of grafted copolymers and the molecular weight of grafted copolymers on the properties of SAN/PPE 40/60 blends, two specific functionalized MWCNT containing different molecular weights of grafted P(MMA-*co*-S) copolymers were selected to prepare SAN/PPE composites. For comparison, the composites with pristine MWCNT were also studied. The used MWCNT fillers for preparing SAN/PPE composites are listed in Table 3.

Table 3 Properties of selected MWCNT fillers in SAN/PPE composites

Code	MWCNT fillers	M_n [kg/mol]	Content of grafted copolymers [wt%]	Fraction of PS [%]
SAN/PPE-MWCNT	Pristine MWCNT	---	---	---
SAN/PPE-MWCNT-*CO*-L	MWCNT-*CO*-3h	29.5	30	56
SAN/PPE-MWCNT-*CO*-H	MWCNT-*CO*-7h	74.7	80	56

3.2.1 Theoretical prediction of the localization of pristine MWCNT in SAN/PPE blends

Regarding to the state of pristine MWCNT in immiscible blends, the selectivity of MWCNT localization is generally explained as a result of thermodynamic equilibrium of the MWCNT fillers in the blends, which can be described by the wetting coefficient ω_α [5, 6, 8, 10]. The

wetting coefficient is defined as a simple mathematical function of interfacial tension [48] and can be adapted to SAN/PPE blends as:

$$\omega_\alpha = \frac{\gamma_{CNT-SAN} - \gamma_{CNT-PPE}}{\gamma_{SAN-PPE}} \quad (2)$$

where γ are the interfacial tensions of the different components. Three cases can be distinguished: If ω_α < -1, CNT are assumed to be located in the first phase (SAN). If ω_α > 1, CNT are predicted to be in the second phase (PPE). If -1 < ω_α < 1, CNT are presumed to concentrate at the interface between the two components.

The interfacial tension between different materials can be calculated based on the surface tension of each component using the harmonic-mean equation [49]

$$\gamma_{12} = \gamma_1 + \gamma_2 - 4\left(\frac{\gamma_1^d \gamma_2^d}{\gamma_1^d + \gamma_2^d} + \frac{\gamma_1^p \gamma_2^p}{\gamma_1^p + \gamma_2^p}\right) \quad (3)$$

and the geometric-mean equation [49]

$$\gamma_{12} = \gamma_1 + \gamma_2 - 2\left(\sqrt{\gamma_1^d \gamma_2^d} + \sqrt{\gamma_1^p \gamma_2^p}\right) \quad (4)$$

where γ_1, γ_2 are the surface tensions of the components 1 and 2; γ_1^d, γ_2^d are the dispersive parts of the surface tension of components 1 and 2; γ_1^p, γ_2^p are the polar parts of the surface tension of the components 1 and 2. The harmonic-mean equation is considered to be more suitable for materials with low surface tension and the geometric one is valid to estimate the surface tension between materials with high surface tension and materials with low surface tension.

The values of surface tension of SAN, PPE and MWCNT at 260 °C are listed in Table 4. Because of the high viscosity of PPE, no literature has reported experimental data of the surface tension of PPE in the melt. In this text, we estimated the surface tension of pure PPE at high temperature according to the theoretical study of Everaert et al. [50].

Table 4 Surface tension of the polymers and MWCNT at 260 °C

Material	Total surface tension (γ, mJ·m^{-2})	Dispersive surface tension (γ^d, mJ·m^{-2})	Polar surface tension (γ^p, mJ·m^{-2})	Reference
MWCNT	27.8	17.6	10.2	[51]
MWCNT	45.3	18.4	26.7	[52]
SAN	29.5	22.4	7.1	[5]
PPE	28.4	22.2	6.2	[50], [53]

Table 5 Interfacial tension at 260 °C calculated from harmonic and geometric mean equations

Material	Interfacial tension according to harmonic-mean equation (mJ·m^{-2})	Interfacial tension according to geometric-mean equation (mJ·m^{-2})
SAN/PPE	0.06	0.04
SAN/MWCNT [51]	1.13	0.58
SAN/MWCNT [52]	11.72	6.44
PPE/MWCNT [51]	1.51	0.80
PPE/MWCNT [52]	13.10	7.32

Two different values of surface tension are widely accepted for MWCNT [5, 14, 54]. Nuriel et al. [51] measured the surface tension of MWCNT with a diameter of approx. 30 nm. The values from their study are 45.3 mJ·m^{-2} for the total surface tension, while, 18.4 mJ·m^{-2} and 26.9 mJ·m^{-2} for dispersive and polar surface tension, respectively. Barber et al. [52] applied atomic force microscopy and a Wilhelmy balance method to quantify the contact angle between MWCNT and different organic liquids. The measured nanotubes were grown by arc-discharge with a diameter of approx. 20 nm. The total surface tension of MWCNT in their study was 27.8 mJ·m^{-2} with a dispersive component of 17.6 mJ·m^{-2} and a polar component of 10.2 mJ·m^{-2}. Since the diameter of MWCNT varies, these two typical data are both adapted in our estimation. On the basis of these data, the calculated interfacial tensions are listed in Table 5 and the corresponding wetting coefficient values are given in Table 6.

Table 6 Wetting coefficient estimated according to the harmonic-mean and the geometric-mean equations

System	ω_a (harmonic-mean equation)	ω_a (geometric-mean equation)
SAN/PPE/MWCNT [51]	-6.33	-5.50
SAN/PPE/MWCNT [52]	-23.00	-22.00

The wetting coefficient is negative in all cases, because the interfacial tensions between SAN and MWCNT are lower than the ones involving PPE. This marginal difference of the interfacial tensions should be sufficient to promote the location of MWCNT in the preferable phase in thermodynamic equilibrium [12]. Consequently, according to the aforementioned estimation, the localization of MWCNT in SAN/PPE blends is predicted to be in the SAN phase which has a better affinity with MWCNT.

However, Fenouillot et al. [55] and Göldel et al. [56] declared in their recent studies that the effect of thermodynamic interaction in the systems can be hampered by a very high polymer viscosity, especially in immiscible blends where the two components have significantly different viscosities. In their works, pristine MWCNT fillers were found to be favorable with the phase with lower viscosity where they can diffuse more rapidly. Thus, it is essential to take into account the influence of viscosity. In SAN/PPE blends, referring to our previous measurements of the used materials under the same processing conditions [43], the SAN component (η_0= 900 Pas) is much less viscous than the PPE component (η_0= 45600 Pas) at 260 °C. Therefore, even only considering the effect of viscosity, MWCNT would be still presumed to disperse selectively in the SAN phase, but neither in the PPE phase nor at the interface of the blends.

3.2.2 Influence of molecular weight of grafted copolymers on the localization of MWCNT fillers in immiscible SAN/PPE 40/60 blends

In our previous study, we demonstrated that the molecular weight of grafted homopolymer has a significant effect on the localization of MWCNT in SAN/PPE blends [43]. In this work, although no pre-mixing procedure was applied, different locations MWCNT fillers are expected when varying the molecular weight of grafted copolymers.

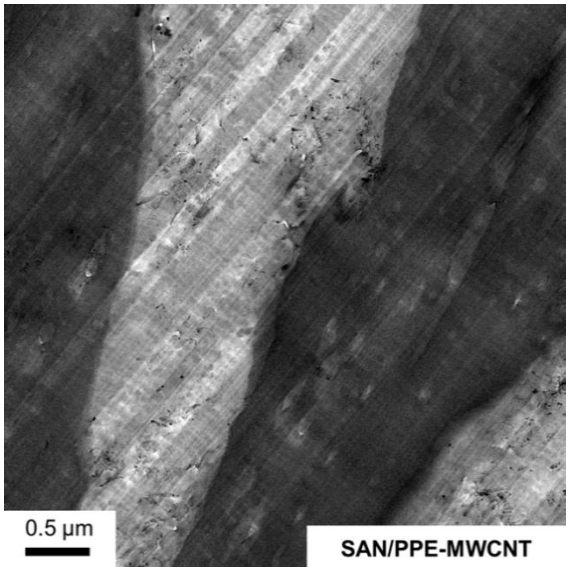

(a)

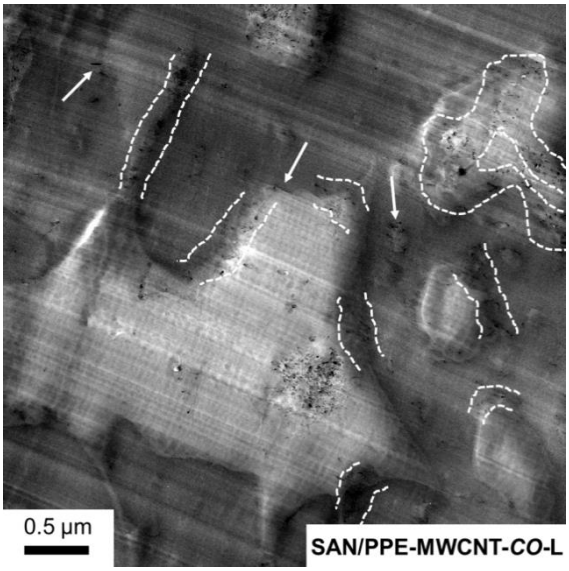

(b)

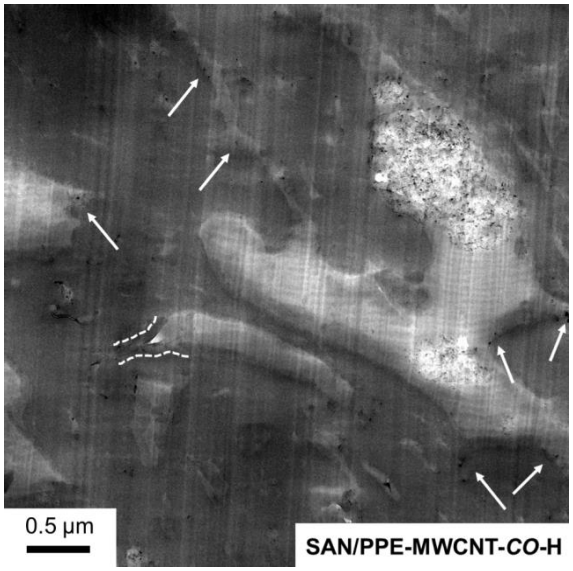

(c)

Fig. 6 TEM micrographs of SAN/PPE 40/60 blends filled with various MWCNT fillers: SAN/PPE-MWCNT (a), SAN/PPE-MWCNT-*CO*-L (b) and SAN/PPE-MWCNT-*CO*-H (c). The MWCNT locating at the interface are highlighted by the pairs of dashed lines and the arrows.

Transmission electron micrographs of SAN/PPE 40/60 blends filled with different MWCNT fillers are shown in Fig. 6. The PPE phase appears as grey and the SAN phase shows as bright regions. As can be seen in Fig. 6(a), almost all pristine MWCNT are initially located in the bright SAN phase. Only very few tubes can be found in the PPE phase. This micrograph confirms the prediction evaluated from the wetting coefficient and viscosity ratio of SAN and PPE (see Section 3.2.1). A similar phenomenon was also observed in our previous work, where the

MWCNT were premixed with SAN before blending with PPE [43].

In contrast to pristine MWCNT, the location of functionalized MWCNT with grafted polymers does not only depend on the interfacial tension between pristine MWCNT and the components of blends, but is also influenced by the thermodynamic relationship between the blend components and the grafted polymer. Many examples revealed that a thermodynamic equilibrium of the blends and the grafted polymer can provide a driving force to confine the localization of CNT in a particular phase or at the interface [13, 17, 43, 57]. In our system, PS has a driving force to enter into the PPE phase ($\chi_{PPE/PS}$ = -0.1) [58] and PMMA should enter in the SAN phase ($\chi_{SAN/PMMA}$ = -0.008) [24, 58]. Thus, P(MMA-*co*-S) copolymers on the surface of MWCNT may promote the localization of MWCNT at the interface of SAN/PPE blends. This assumption is confirmed by the TEM results shown in Fig. 6(b). In the micrograph, many functionalized MWCNT are found to arrange at the interface of the blends (highlighted by white dashed lines and arrows). This localization is more pronounced at the boundary between the continuous PPE phase and the small SAN droplets. However, the distribution of MWCNT is not perfectly uniform. A small fraction of single tubes are observed in the PPE phase and a few agglomerates can be also seen in the SAN phase nearby the interface. Possible reasons for the location in the PPE phase could be attributed to the lower χ parameter between PPE and PS that implies a stronger driving force to promote MWCNT in the PPE phase. In addition, the slightly higher PS content in the grafted copolymers (56%) is another reason for the tendency of localization in the PPE phase.

When the molecular weight of grafted polymer increases, the aggregation of MWCNT becomes more evident, which is demonstrated by the large agglomerates in Fig. 6(c). The investigation of the pristine polymer system without CNT reveals that the compatibilizer with high molecular weight or an extra amount of compatibilizers can lead to micellization of copolymers in multi-phase systems [18, 24]. For SAN/PPE-MWCNT-*CO*-H, the molecular weight of grafted P(MMA-*co*-S) copolymers is 74.7 kg/mol, which is more than twice of the value in the sample of SAN/PPE-MWCNT-*CO*-L (see Table 3). Thus, increasing agglomeration possibly originates from the tendency of micellization of high molecular weight copolymers covering the surface of MWCNT. Additionally, as the content of neat MWCNT is equal for all samples, increasing

molecular weight consequently causes an increasing content of grafted polymers, which can strengthen the effect of micellization leading to a more pronounced agglomeration of functionalized MWCNT.

In this study, no indication of the effect of "autophobic dewetting" can be observed [59-61]. It was shown in several works that the matrix polymer wets the polymer brush if the molecular weight of the matrix is less than the molecular weight of the grafted copolymer [58, 62, 63]. In our work a copolymer was grafted on the MWCNT. The entropy is determined by the total length of the copolymer chain. Since the molecular weights of the grafted copolymers are larger than the molecular weight of the PPE phase, our experimental results are in agreement with the phenomenon of autophobic dewetting. In our systems, the relatively low value of χ parameter for PPE/PS promotes localization of MWCNT at the interphase between SAN and PPE. The large agglomerates in the SAN phase in case of the high molecular weight graft copolymer result from a functionalization of the whole agglomerate (and not of the individual tubes). In this case, the volume of the agglomerate is very large and therefore diffusion into the thermodynamically more favorable PPE phase takes places very slowly. The agglomerates are located in the SAN phase because the SAN pellets “melt” earlier than PPE during extrusion and hence the MWCNT are mixed into the SAN phase in the early stage of mixing.

3.2.3 The influence of molecular weight of grafted copolymers on the morphology of SAN/PPE blends

As discussed above, the localization of MWCNT fillers is significantly influenced by the molecular weight of grafted P(MMA-*co*-S) copolymers on their surface. Due to this variation of location, the morphology of SAN/PPE 40/60 blends also changes. In Fig. 7, the morphology of SAN/PPE 40/60 blends and its composites with various MWCNT fillers are shown.

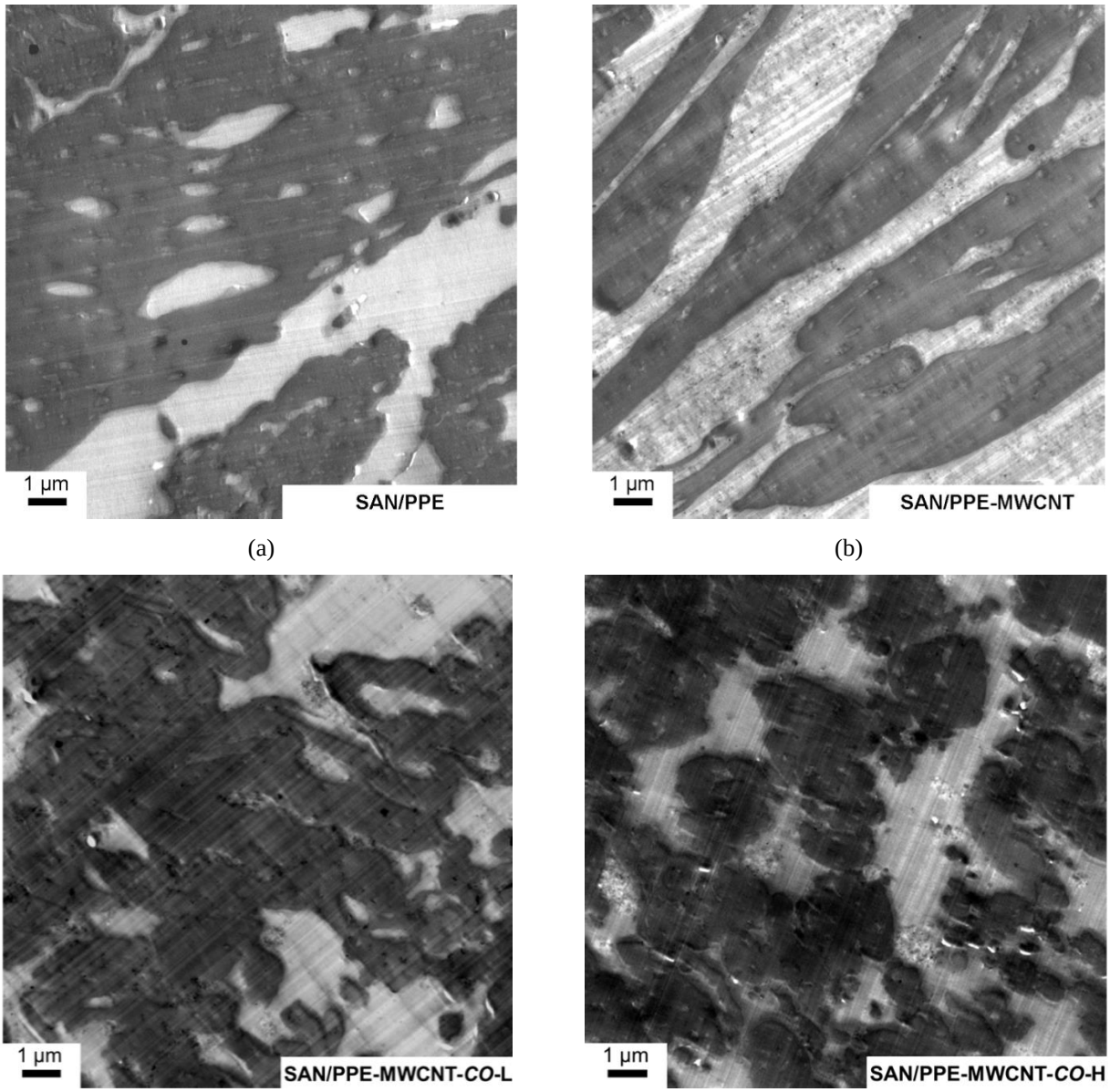

Fig. 7 Morphology of SAN/PPE 40/60 blends and its composites with various MWCNT fillers: SAN/PPE (a), SAN/PPE-MWCNT (b), SAN/PPE-MWCNT-*CO*-L (c) and SAN/PPE-MWCNT-*CO*-H (d)

In the TEM micrograph of the neat SAN/PPE blends (see Fig. 7(a)), PPE forms the continuous phase. The main fraction of SAN is continuous and many small inclusions of SAN are dispersed in PPE. After filling with pristine MWCNT, both the SAN and the PPE phase present a high continuity and the size of SAN droplets in PPE significantly decreases (see Fig. 7(b)). This change of morphology can be explained by the change of the viscosity ratio between the two blend components. The selective location of fillers in SAN enhances the viscosity of the SAN phase, leading to an obvious increase of continuity of the SAN phase. When MWCNT fillers are

functionalized with P(MMA-*co*-S) copolymers, MWCNT transfer from the SAN phase to the interface, while some MWCNT are dispersed in the PPE phase. Consequently, the morphology of SAN/PPE composites are found to vary with functionalization of MWCNT. In the case of SAN/PPE-MWCNT-*CO*-L, the breakup of the continuous PPE phase is observed in Fig. 7(c). With increasing molecular weight of grafted P(MMA-*co*-S) copolymers, the continuity of the PPE phase is considerably disrupted and turned into droplets which are dispersed in the continuous SAN phase. This apparent variation of morphology might be related to the softening effect of grafted copolymer and the change of the viscosity ratio between the two components in the melt. The effect is more pronounced when more MWCNT locate in the PPE phase with a higher copolymer content.

3.2.4 Rheological properties of SAN/PPE 40/60 blends filled with MWCNT

In order to further elucidate the influence of MWCNT on the microstructure of SAN/PPE blends, the rheological properties of SAN/PPE blends filled with various MWCNT are analyzed by comparing them with the neat blend. The frequency dependence of the storage modulus, the loss modulus and the complex viscosity of neat SAN/PPE 40/60 blends and its composites are presented in double logarithmic scales in Fig. 8.

Since the storage modulus at low frequencies is very sensitive to the microstructure of the materials, a remarkable difference between the neat SAN/PPE blends and the composites is clearly demonstrated in Fig. 8(a), even if the effective loading of MWCNT in each sample is only 1 wt%. The slope of G' for the neat SAN/PPE blends is lower than 2 with a value of approx. 0.5. After adding pristine MWCNT, the slope of SAN/PPE-MWCNT is further decreased with a higher storage modulus at low frequencies. The TEM micrograph in Fig. 6(a) shows that most pristine MWCNT are selectively located in the SAN phase. Thus, the increase of G' by addition of pristine MWCNT should be a response of the reinforcement of SAN phase caused by the elasticity of the MWCNT and elastic MWCNT-MWCNT interactions [64, 65], which is generally observed for polymer composites filled with CNT [66-69].

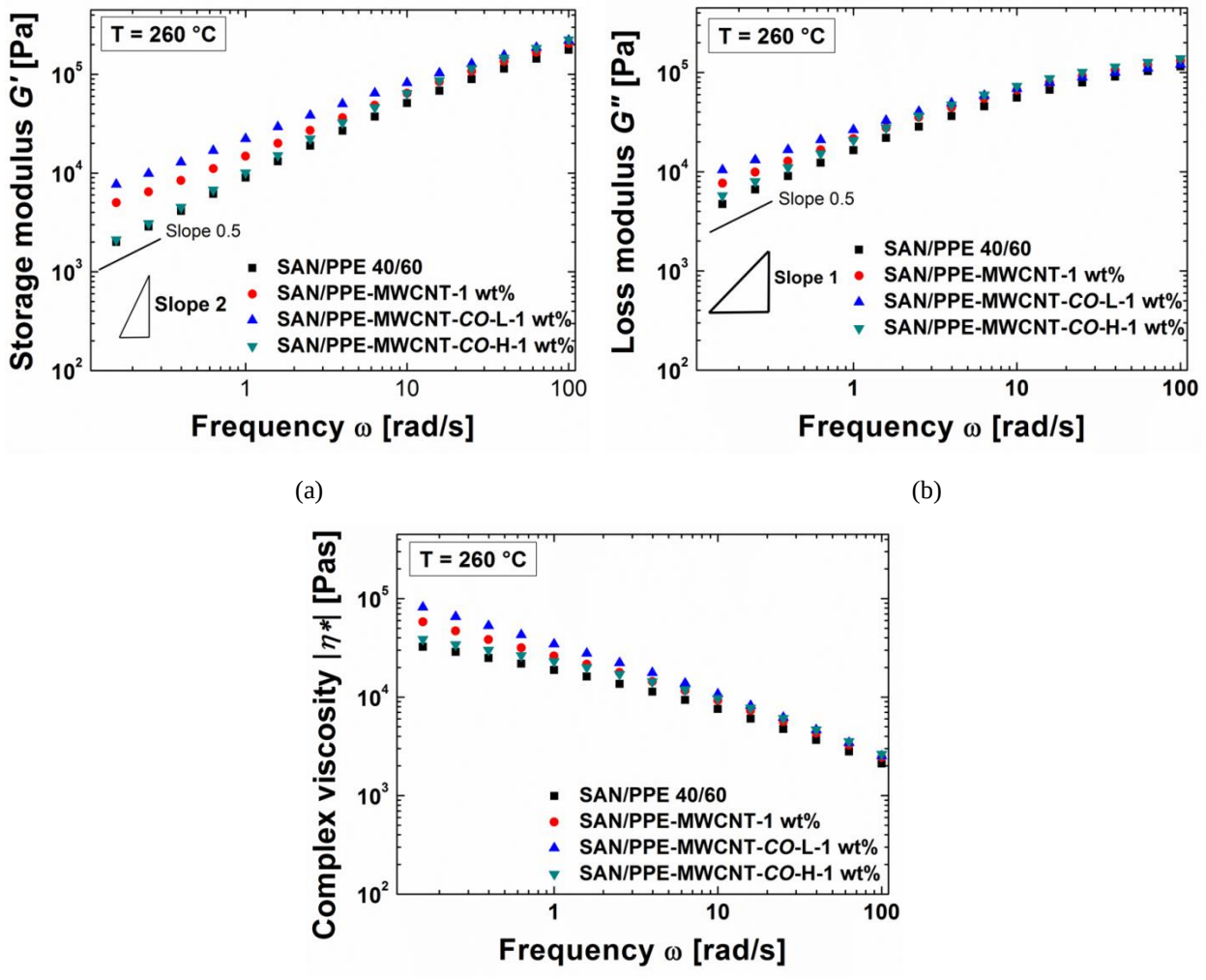

Fig. 8 Storage modulus G' (a), loss modulus G'' (b) and complex viscosity $|\eta^*|$ (c) of SAN/PPE 40/60 blend and its composites with MWCNT fillers as a function of angular frequency ω at 260 °C.

Interestingly, compared to other samples, the composite of SAN/PPE-MWCNT-*CO*-L presents the highest storage modulus at low frequencies. A slight increase of the loss modulus and the complex viscosity are also observed in Figs. 8(b) and (c). The increase of dynamic moduli and viscosity could be a result of formation of nanotubes network due to the localization of MWCNT. In contrast to the random dispersion of pristine MWCNT with a visible and long distance between two tubes in the SAN phase, functionalized MWCNT locate along the interface of the blends and are partially in contact with each other, even if it is only observed in some fraction of the interface. Therefore, in these regions, the CNT-CNT interactions are enhanced [9], which are one contribution to the increase of elasticity of the composites. Nevertheless, such influence is overcome by the softening effect of grafted copolymers when the molecular weight of

P(MMA-*co*-S) copolymers increases to a high level, which is indicated by the rheological properties of the sample SAN/PPE-MWCNT-*CO*-H presenting a similar behavior to the neat SAN/PPE blend with relatively low dynamic moduli and complex viscosity. The change of viscosity ratio of the components is also indicated by the different morphology of the blends in Fig. 8.

The structural changes resulting from the localization of MWCNT are further elucidated by modified Cole-Cole plots (see Fig. 9). The Cole-Cole plots depict a slope of 2 for homopolymers [70-72]. Thus, owing to its multi-phase structure, the slope in the terminal region of the neat SAN/PPE 40/60 blend is less than 2. After addition of pristine MWCNT, the plot distinctively deviates from the curve of the neat blend with larger G' values, which demonstrates the formation of a CNT-CNT network in the SAN phase. The SAN/PPE-MWCNT-*CO*-L composite is associated with a similar slope as the composite with pristine MWCNT. However, the curve of SAN/PPE-MWCNT-*CO*-H is similar to the one of the neat blend. It is mainly attributed to the pronounced agglomeration in case of SAN/PPE-MWCNT-*CO*-H. Furthermore, the increased distance between individual nanotubes due to the wrapped polymer layer on the surface of MWCNT also weakens the interactions between MWCNT.

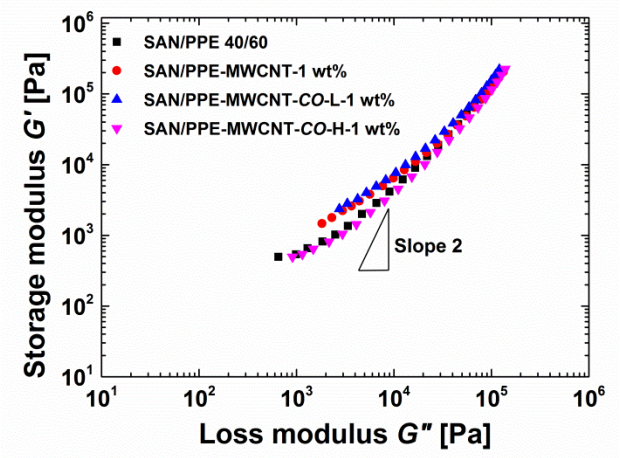

Fig. 9 Modified Cole-Cole plot of SAN/PPE 40/60 blend and its composites with MWCNT

Combining these results, it can be concluded that the molecular weight of grafted copolymer on the surface of MWCNT cannot only control the localization of MWCNT in SAN/PPE blends, but

also has an important influence on the morphological and rheological properties of the composites.

3.2.5 Conductivity and permittivity of SAN/PPE 40/60 blends filled with MWCNT fillers

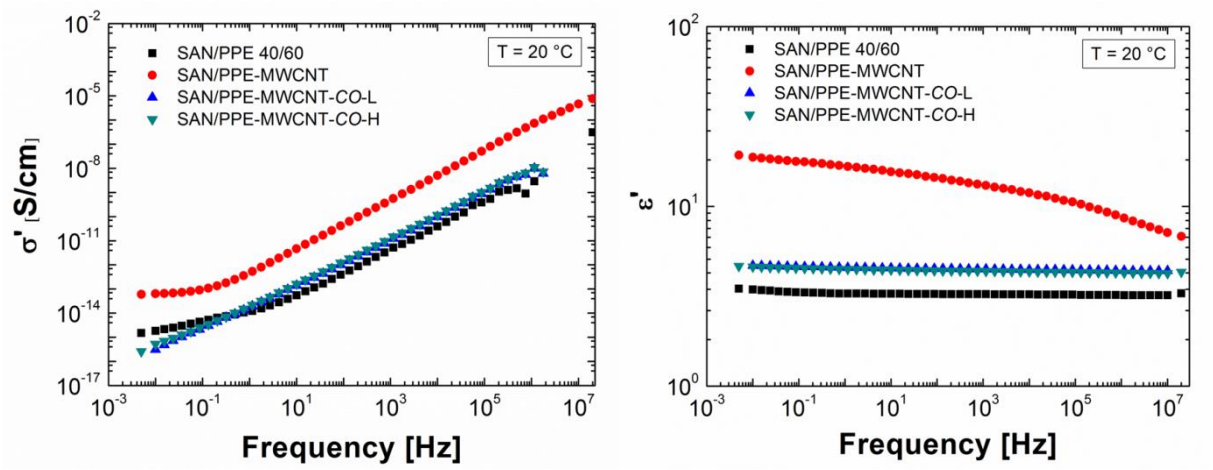

(a) (b)

Fig. 10 AC conductivity δ' (a) and real part of complex permittivity ε' (b) of SAN/PPE 40/60 blend and its composites with MWCNT fillers as a function of frequency at 20 °C.

Since the present samples in our work have a relatively low electrical conductivity which is outside the measurement range of our four-probe device, dielectric spectroscopy was chosen to study the electrical conductivity. As can be seen in Fig. 10(a), the SAN/PPE nanocomposite with pristine MWCNT has a significantly higher conductivity value (e.g. 10^{-13} S/cm at 0.005 Hz) than the neat blend (e.g. 10^{-15} S/cm at 0.005 Hz), since MWCNT cumulate in the SAN phase and have a good geometric and electrical contact with each other because of a network-like structure. The enhancement is larger than for pure SAN and a SAN/MWCNT composite under the same loading [5]. Slight improvement by adding MWCNT into homopolymers was also observed in other composites. In the work of Pötschke et al. [73], the DC conductivity of PC composites with 1 wt% MWCNT was measured at low frequencies (lower than 10^{-4} Hz) and was 10^{-16} S/cm similar to the neat PC. Thus, in our system, the enhancement of electrical conductivity substantially reflects the decrease of the percolation threshold due to the double percolation. However, in this work, MWCNT loading of the composites does not reach the percolation threshold, which is indicated by a missing direct conductivity (DC) plateau at low frequencies which can be found for

nanocomposites above the percolation threshold [66, 73].

For the composites with functionalized MWCNT, the conductivity values show a behavior similar to the neat SAN/PPE blend (e.g. 10^{-15} S/cm at 0.005 Hz), which is much smaller than the one with pristine MWCNT. Moreover, as no limiting constant value was detected at low frequencies, a DC value cannot be defined. It is well known that a three dimensional network formed by CNT is necessary to enhance the electrical conductivity [74, 75]. However, as shown in the TEM micrographs (Fig. 6), functionalized MWCNT spread not only at the interface but also in the PPE phase which has a low conductivity. Moreover, some fractions agglomerate into bundles. Consequently, no continuous nanotube-nanotube network can be formed to achieve a high conductivity because of the diverse localization of functionalized MWCNT. Last but not least, compared to pristine MWCNT, more defects on the surface of functionalized MWCNT might be another reason leading to an reduction of electrical conductivity due to the collisions between electron and defects which deflect the electron from its path [76].

Although there is no pronounced enhancement of electrical conductivity in the composites with functionalized MWCNT, an increase of dynamic moduli of SAN/PPE-MWCNT-*CO*-L was observed (see Fig. 8). This phenomenon has also been observed in other composites [74], which should be mainly attributed to the different physical mechanisms for electrical conductivity and rheological properties [66, 75]. The rheological properties of the composites are mainly determined by the combination of the entangled polymer network, the nanotubes-polymer network, the MWCNT-MWCNT interactions and the elasticity of the nanotubes. In particular, the MWCNT-MWCNT interactions are influenced of the state of dispersion of nanotubes. The dielectric data indicate that MWCNT mainly increase the electrical conductivity if they are located in the SAN phase, but not at the interface or in the PPE phase when it was functionalized with copolymers.

In agreement with the Kramers-Kronig relation and the proportional relationship between AC conductivity and imaginary part of complex permittivity, the same information can be gathered from the permittivity plots (Fig. 10(b)) as from the conductivity plots (Fig. 10(a)). In the case of neat blends, the values remain frequency independent as an insulating material. A pronounced

decrease of ε' with frequency is observed in the plots of SAN/PPE-MWCNT, implying an increased conductivity. However, the descent of the plot is strictly linear, illustrating that the loading of MWNCT is lower than the critical value of percolation threshold. In case of the composites with functionalized MWCNT, the permittivity of each sample is similar to the neat blends.

4. Conclusions

In this work, MWCNT were successfully functionalized with P(MMA-*co*-S) copolymers via an ATRP reaction. The reactions for grafting copolymers were characterized by a good controllability, such that the random copolymers with different molecular weights were grafted on the surface of MWCNT by adjusting the reaction time.

TEM micrographs indicated a significant influence of grafted copolymers on the localization of MWCNT in SAN/PPE 40/60 blends. The pristine MWCNT were found to be selectively located in the SAN phase, which was in agreement with theoretical predictions. After functionalizing with P(MMA-*co*-S) copolymers, MWCNT were preferentially located at the interface of the blends or in the PPE phase. The localization of nanofillers significantly depended on the molecular weight of grafted copolymers on their surface. In the case of a low molecular weight, a large fraction of functionalized MWCNT was observed at the interface. With increasing molecular weight of P(MMA-*co*-S) copolymer, more MWCNT fillers were confined in the PPE phase. Furthermore, pronounced agglomeration was observed nearby the phase boundary of the blend due to micellization of the high molecular weight of grafted P(MMA-*co*-S) copolymers covering MWCNT. Consequently, the morphology of SAN/PPE varies with different localization of MWCNT.

The influence of functionalized MWCNT on the microstructure of the blends was also detected by rheological and dielectric measurements. The presence of pristine MWCNT remarkably increased the dynamic moduli and the complex viscosity of SAN/PPE blends. These values increased when MWCNT were functionalized with low molecular weight P(MMA-*co*-S) copolymers, as CNT-CNT interaction was improved due to the well contacting MWCNT at the

interface. However, with increase of molecular weight, the composites showed a behavior similar to the neat blends, which was attributed to the softening effect of the grafted copolymers. From the results of dielectric measurements, although the addition of pristine MWCNT was found to considerably enhance the conductivity of the composites even at low loading (1 wt%), little improvement was achieved in the cases of the SAN/PPE composites with functionalized MWCNT. No complete conductive network formed by nanotubes and the location in the PPE phase is probably the main reason for the low conductivity.

In conclusion, the grafting of P(MMA-*co*-S) copolymers with appropriate molecular weight on the surface of MWCNT can be a feasible approach to confine MWCNT at the interface of SAN/PPE blends owing to the thermodynamic interaction between the grafted copolymers and the components of the blends. However, no matter where MWCNT were located, a network-like structure of MWCNT with well contacting among tubes was essential to enhance the dynamic moduli and the complex viscosity as well as the electrical conductivity of the composites. Furthermore, it is worth noting that the high content of grafted polymer on MWCNT resulting from a large molecular weight led to a reduction of both rheological properties and electrical conductivity.

Acknowledgement

This work was financially supported by the 7th Framework Program research EU-project "HARCANA" (Grant Agreement No: NMP3-LA-2008-213277). The authors thank Maren Brinkmann for GPC measurements, Silvio Neumann for ^{1}H-NMR measurements, Dr. Prokopios Georgopanos, Ivonne Ternes and Berthold Wendland for experimental support. We are also grateful to BASF SE (Ludwigshafen, Germany) and FutureCarbon GmbH (Bayreuth, Germany) for kindly supplying SAN and MWCNT, respectively.

References

1. Elias L, Fenouillot F, Majesté JC, Alcouffe P, and Cassagnau P. Polymer 2008;49(20):4378-4385.
2. Sinha Ray S and Bousmina M. Macromolecular Rapid Communications 2005;26(20):1639-1646.

3. Chen G, Lu J, and Wu D. Materials Chemistry and Physics 2007;104(2–3):240-243.
4. Ajayan PM, Stephan O, Colliex C, and Trauth D. Science 1994;265(5176):1212-1214.
5. Göldel A, Kasaliwal G, and Pötschke P. Macromolecular Rapid Communications 2009;30(6):423-429.
6. Pötschke P, Pegel S, Claes M, and Bonduel D. Macromolecular Rapid Communications 2008;29(3):244-251.
7. Li Y and Shimizu H. Macromolecules 2008;41(14):5339-5344.
8. Wu M and Shaw L. Journal of Applied Polymer Science 2006;99(2):477-488.
9. Wu D, Zhang Y, Zhang M, and Yu W. Biomacromolecules 2009;10(2):417-424.
10. Sun Y, Guo Z, and Yu J. Macromolecular Materials and Engineering 2010;295(3):263-268.
11. Zou H, Wang K, Zhang Q, and Fu Q. Polymer 2006;47(22):7821-7826.
12. Krasovitski B and Marmur A. The Journal of Adhesion 2005;81(7-8):869-880.
13. Tao F, Nysten B, Baudouin AC, Thomassin JM, Vuluga D, Detrembleur C, and Bailly C. Polymer 2011;52(21):4798-4805.
14. Baudouin AC, Devaux J, and Bailly C. Polymer 2010;51(6):1341-1354.
15. Bose S, Bhattacharyya AR, Kodgire PV, Misra A, and Pötschke P. Journal of Applied Polymer Science 2007;106(5):3394-3408.
16. Bose S, Bhattacharyya AR, Kodgire PV, and Misra A. Polymer 2007;48(1):356-362.
17. Chen J, Shi YY, Yang JH, Zhang N, Huang T, and Wang Y. Polymer 2013;54(1):464-471.
18. Lee MS, Lodge TP, and Macosko CW. Journal of Polymer Science Part B: Polymer Physics 1997;35(17):2835-2842.
19. Dai CA, Dair BJ, Dai KH, Ober CK, Kramer EJ, Hui CY, and Jelinski LW. Physical Review Letters 1994;73(18):2472-2475.
20. Cho K, Tae Oan A, Hyun Soo R, and Kyung Hoon S. Polymer 1996;37(21):4849-4852.
21. Roe RJ and Rigby D. Phase relations and miscibility in polymer blends containing copolymers. Polymer Physics, vol. 82: Springer Berlin Heidelberg, 1987. pp. 103-139.
22. Lyatskaya Y, Gersappe D, Gross NA, and Balazs AC. The Journal of Physical Chemistry 1996;100(5):1449-1458.
23. Ruckdäschel H, Sandler JKW, Altstädt V, Schmalz H, Abetz V, and Müller AHE. Polymer 2007;48(9):2700-2719.
24. Ruckdäschel H, Sandler JKW, Altstädt V, Rettig C, Schmalz H, Abetz V, and Müller AHE. Polymer 2006;47(8):2772-2790.
25. Kirschnick T, Gottschalk A, Ott H, Abetz V, Puskas J, and Altstädt V. Polymer 2004;45(16):5653-5660.
26. Krause B, Mende M, Pötschke P, and Petzold G. Carbon 2010;48(10):2746-2754.
27. FutureCarbon. Product information. 2009.
28. Ryu J, Ramaraj B, and Yoon KR. Surface and Interface Analysis 2009;41(4):303-309.
29. Liu H, O'Mahony CT, Audouin F, Ventura C, Morris M, and Heise A. Macromolecular Chemistry and Physics 2012;213(1):108-115.
30. Becer CR, Hoogenboom R, Fournier D, and Schubert US. Macromolecular Rapid Communications 2007;28(10):1161-1166.
31. Dayananda K and Dhamodharan R. Journal of Polymer Science Part A: Polymer Chemistry 2004;42(4):902-915.
32. Matyjaszewski K, Wang JL, Grimaud T, and Shipp DA. Macromolecules 1998;31(5):1527-1534.
33. Sun X, Zhang H, Huang X, Wang X, and Zhou QF. Polymer 2005;46(14):5251-5257.
34. Wang S, Liang Z, Liu T, Wang B, and Zhang C. Nanotechnology 2006;17(6):1551-1557.

35. Lee YW, Kang S, Yoon K, Chi Y, Choi I, Hong SP, Yu BC, Paik HJ, and Yun W. Macromolecular Research 2005;13(4):356-361.
36. Wang TL and Tseng CG. Journal of Applied Polymer Science 2007;105(3):1642-1650.
37. Osswald S, Havel M, and Gogotsi Y. Journal of Raman Spectroscopy 2007;38(6):728-736.
38. Albuerne J, Boschetti-de-Fierro A, and Abetz V. Journal of Polymer Science Part B: Polymer Physics 2010;48(10):1035-1046.
39. Zenkel C, Albuerne J, Emmler T, Boschetti-de-Fierro A, Helbig J, and Abetz V. Microchimica Acta 2012;179(1-2):41-48.
40. Baskaran D, Dunlap JR, Mays JW, and Bratcher MS. Macromolecular Rapid Communications 2005;26(6):481-486.
41. Yang JC, Jablonsky MJ, and Mays JW. Polymer 2002;43(19):5125-5132.
42. Wang Y, Teng X, Wang JS, and Yang H. Nano Letters 2003;3(6):789-793.
43. Du B, Handge UA, Majeed S, and Abetz V. Polymer 2012;53(24):5491-5501.
44. Gao C, Muthukrishnan S, Li W, Yuan J, Xu Y, and Müller AHE. Macromolecules 2007;40(6):1803-1815.
45. Kotani Y, Kamigaito M, and Sawamoto M. Macromolecules 1998;31(17):5582-5587.
46. Brar AS and Puneeta. Journal of Polymer Science Part A: Polymer Chemistry 2006;44(6):2076-2085.
47. Young L. In: Brandrup J and Immergut E, editors. Polymer Handbook. New York: Wiley, 1989.
48. Sumita M, Sakata K, Asai S, Miyasaka K, and Nakagawa H. Polymer Bulletin 1991;25(2):265-271.
49. Wu S. Journal of Macromolecular Science, Part C 1974;10(1):1-73.
50. Everaert V, Groeninckx G, Pionteck J, Favis BD, Aerts L, Moldenaers P, and Mewis J. Polymer 2000;41(3):1011-1025.
51. Nuriel S, Liu L, Barber AH, and Wagner HD. Chemical Physics Letters 2005;404(4–6):263-266.
52. Barber AH, Cohen SR, and Wagner HD. Physical Review Letters 2004;92(18):186103.
53. http://www.accudynetest.com/polytable_01.html.
54. Zhang L, Wan C, and Zhang Y. Polymer Engineering & Science 2009;49(10):1909-1917.
55. Fenouillot F, Cassagnau P, and Majesté JC. Polymer 2009;50(6):1333-1350.
56. Göldel A, Kasaliwal GR, Pötschke P, and Heinrich G. Polymer 2012;53(2):411-421.
57. Liu L, Wang Y, Li Y, Wu J, Zhou Z, and Jiang C. Polymer 2009;50(14):3072-3078.
58. Auschra C and Stadler R. Macromolecules 1993;26(24):6364-6377.
59. Shull KR. The Journal of Chemical Physics 1991;94(8):5723-5738.
60. Clarke CJ, Jones RAL, Edwards JL, Shull KR, and Penfold J. Macromolecules 1995;28(6):2042-2049.
61. Laub CF and Koberstein JT. Macromolecules 1994;27(18):5016-5023.
62. Noolandi J and Hong KM. Macromolecules 1982;15(2):482-492.
63. Bucknall DG, Higgins JS, and Rostami S. Polymer 1992;33(20):4419-4422.
64. Handge UA, Zeiler R, Dijkstra D, Meyer H, and Altstädt V. Rheologica Acta 2011;50(5-6):503-518.
65. Zeiler R, Handge UA, Dijkstra DJ, Meyer H, and Altstädt V. Polymer 2011;52(2):430-442.
66. Pötschke P, Abdel-Goad M, Alig I, Dudkin S, and Lellinger D. Polymer 2004;45(26):8863-8870.
67. Sung YT, Han MS, Song KH, Jung JW, Lee HS, Kum CK, Joo J, and Kim WN. Polymer 2006;47(12):4434-4439.
68. Lee SH, Cho E, Jeon SH, and Youn JR. Carbon 2007;45(14):2810-2822.
69. Kim JA, Seong DG, Kang TJ, and Youn JR. Carbon 2006;44(10):1898-1905.
70. Han CD and Kim J. Journal of Polymer Science Part B: Polymer Physics 1987;25(8):1741-1764.
71. Pötschke P, Fornes TD, and Paul DR. Polymer 2002;43(11):3247-3255.
72. Ko SW, Gupta RK, Bhattacharya SN, and Choi HJ. Macromolecular Materials and Engineering

2010;295(4):320-328.
73. Pötschke P, Dudkin SM, and Alig I. Polymer 2003;44(17):5023-5030.
74. Cohen E, Zonder L, Ophir A, Kenig S, McCarthy S, Barry C, and Mead J. Macromolecules 2013;46(5):1851-1859.
75. Hu G, Zhao C, Zhang S, Yang M, and Wang Z. Polymer 2006;47(1):480-488.
76. Khare R and Bose S. Journal of Minerals & Materials Characterization & Engineering 2005;4(1):31-46.